A Monte Carlo study of pressure dependent effects in the electron impact excitation of the He 3^1P state

2000 Meas. Sci. Technol. 11 1193

(http://iopscience.iop.org/0957-0233/11/8/314)

Meas. Sci. Technol. **11** (2000) 1193–1207. Printed in the UK PII: S0957-0233(00)12057-0

A Monte Carlo study of pressure dependent effects in the electron impact excitation of the He 3^1P state

Ian Humphrey

Daresbury Laboratory, Daresbury, Warrington WA4 4AD, UK

Received 22 February 2000, in final form 18 April 2000, accepted for publication 27 April 2000

Abstract. A preliminary study is presented of pressure dependent effects in the electron impact excitation of the 3^1P state of helium. Only polarization correlations are considered.

Monte Carlo techniques are used. An effort has been made to produce a realistic model of the scattering centre in a crossed beam experiment, and to use an accurate simulation of the absorption and re-emission process. Extensive details of the modelling process and the equations are included.

These early results are in good agreement with the radiation trapping model of Williams *et al*, although the Andersen parameter, P_{lin}, appears to decay more slowly with pressure than expected.

Some notable results include the very rapid decay of some P_4 measurements with pressure, and the insensitivity of the alignment angle to pressure or time of release.

Keywords: Stokes' parameters, photon polarization, electron–photon coincidence, atomic excitation, crossed beams, radiation trapping, alignment, orientation, polarimeter, gas jet, Monte Carlo, pressure, systematic errors, data correction, data analysis

(Some figures in this article are in colour only in the electronic version; see `www.iop.org`)

1. Introduction

It has long been recognized that the finite size and finite pressure of the interaction region influence the results of crossed beam experiments (e.g. Zetner *et al* 1989, 1990, van der Burgt *et al* 1991, Hishikawa *et al* 1992). In atomic coincidence spectroscopy, for example, the divergence between the experimental results from different groups is often well in excess of the differences between the theoretical models the experiments seek to distinguish (Andersen *et al* 1988, McLaughlin *et al* 1994). The goal of the present paper is to explore further how real experimental conditions modify the results of the ideal experiment.

Some recent studies of pressure dependence (e.g. Wang *et al* 1998) include simplifying assumptions such as uniform target gas density and interaction regions confined to simple geometric boundaries. This paper describes a more realistic model of the scattering centre. The gas jet is assumed to be an effusive or slightly modified effusive source, the electron beam has a Gaussian intensity profile and the detector is defined by the passage of rays through two circular apertures.

With enough knowledge of the gas, electron beam and detector characteristics, the expected result of an experiment can be calculated from the theoretical parameters. However, this involves a difficult integration over many degrees of freedom. To ensure an accurate result, the step size would have to be small, and the total number of integration steps prohibitively large. To reduce this computational expense one might seek instead to simulate the physical process itself by sampling all the probability distributions implicitly involved in the integrating process. A small number of integrating points then implies not a wrong result but a result that would be obtained in an experiment with poor statistics. This probabilistic approach is known as the Monte Carlo method. The Monte Carlo method is a way of reproducing physical processes by representing them as a series of choices, and it is a very efficient way of integrating over a multi-dimensional parameter space. This is why the Monte Carlo approach has been adopted for the current study.

2. Theory

2.1. Absorption and emission of radiation

To conduct the simulation it is necessary to examine how the chain of emission, absorption and re-emission affects the polarization state of a photon. The reader is referred to a book by Blum (1996) for a thorough treatment of what is only adumbrated here. The weak field approximation is assumed.

2.1.1. Emission of radiation from an atom in a known state. The photon polarization density matrix of the field of spontaneously emitted photons,

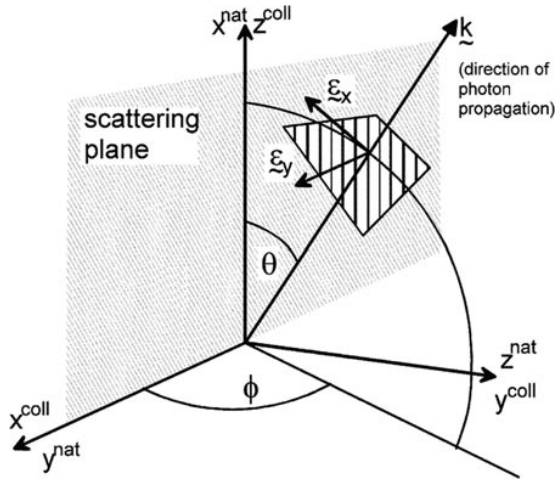

Figure 1. The co-ordinates used in the text. 'coll' denotes collision frame axes, and 'nat' denotes natural frame axes (Andersen *et al* 1988). ε_x and ε_y refer to the polarization unit vectors mentioned in the text, and $\boldsymbol{k}$ is the Poynting vector of the photon. The scattering plane is defined by the direction of propagation of the incoming electrons, z^{coll}, and the direction of propagation of the scattered electrons.

$\rho^{emission,\ photon\ frame}$, is related to the excited atomic density matrix, $\rho^{atom,\ collision\ frame}$, by the fluorescence operator, F.

$$\rho^{emission,\ photon\ frame}_{\lambda',\lambda} = F_{\lambda',\lambda}\rho^{atom,\ collision\ frame} \equiv \sum_{M_2',M_2} F^{M_2',M_2}_{\lambda',\lambda}\rho^{atom,\ collision\ frame}_{M_2',M_2} \tag{2.1.1}$$

where the elements of the fluorescence operator are given by

$$F^{M_2',M_2}_{\lambda',\lambda}(R) \propto (-1)^{M_2'-M_2}\sum_{M_1} D^1_{(M_2'-M_1),\lambda'}(R)D^{1*}_{(M_2-M_1),\lambda}(R) \times \begin{pmatrix} J_1 & 1 & J_2 \\ -M_1 & M_1-M_2' & M_2' \end{pmatrix} \times \begin{pmatrix} J_1 & 1 & J_2 \\ -M_1 & M_1-M_2 & M_2 \end{pmatrix}. \tag{2.1.2}$$

In this expression, R is the set of Euler angles representing the rotation from the collision frame to the frame of emission, $R = (\phi, \theta, 0)$, and the symbol D represents the rotation matrices (Brink and Satchler 1994). The proportionality constant is not important here, and depends on various dynamical factors.

The relationships between the polarization density matrix and the Stokes parameters of the light are given by Blum (1996).

Coordinate systems used in this analysis are illustrated in figure 1.

2.1.2. Photon polarization after atomic absorption. A photon with a polarization density matrix $\rho^{incoming\ photon}_{\lambda',\lambda}$ is absorbed by an atom in a state of total angular momentum J_1 and described by the density matrix $\rho^{ground\ state\ atom,\ collision\ frame}_{M_1',M_1}$. The atom is excited to a state of total angular momentum J_2. In relaxation back to the ground state, it releases a photon described by the photon polarization density matrix, $\rho^{outgoing\ photon}_{\lambda',\lambda}$.

The relationship between $\rho^{outgoing\ photon}_{\lambda',\lambda}$ and $\rho^{incoming\ photon}_{\lambda',\lambda}$ is given by equation (2.1.3).

$$\rho^{outgoing\ photon}_{\lambda',\lambda} \propto \sum_{\substack{M_2',M_2\\M_1',M_1\\M_1''\\\Lambda',\Lambda}} D^{1*}_{(M_2'-M_1''),\lambda'}(R_2)D^1_{(M_2-M_1''),\lambda}(R_2) \times D^{1*}_{(M_2-M_1),\Lambda}(R_1)D^1_{(M_2'-M_1'),\Lambda'}(R_1) \times \begin{pmatrix} J_1 & 1 & J_2 \\ -M_1'' & M_1''-M_2' & M_2' \end{pmatrix} \times \begin{pmatrix} J_1 & 1 & J_2 \\ -M_1'' & M_1''-M_2 & M_2 \end{pmatrix} \times \begin{pmatrix} J_2 & 1 & J_1 \\ -M_2' & M_2'-M_1' & M_1' \end{pmatrix} \times \begin{pmatrix} J_2 & 1 & J_1 \\ -M_2 & M_2-M_1 & M_1 \end{pmatrix} \times \rho^{incoming\ photon}_{\Lambda',\Lambda}\rho^{ground\ state\ atom,\ collision\ frame}_{M_1',M_1}. \tag{2.1.3}$$

In equation (2.1.3), $R_1 = (\phi_1, \theta_1, 0)$ and $R_2 = (\phi_2, \theta_2, 0)$ are the Euler angles representing the rotations from the collision frame to the emission frame for the incoming and outgoing photons respectively.

2.2. Rotating the polarization to the detector frame

As discussed by Humphrey (1999), careful thought has to be given to the relationship between the polarization axes of the radiation and the detector.

In this paper, the model of Humphrey (1999) is slightly modified. An ideal lens is imagined in which all incident rays, regardless of point of origin or angle of incidence, are refracted parallel to the symmetry axis of the lens.

The raw polarizations reported by the Monte Carlo simulation must be corrected so that they report the polarization measured by the ideal lens system.

The corrected polarizations (P_x'), relative to the detector axes, are given in terms of the original polarizations (P_x) relative to the standard polarization unit vectors by equations (2.2.1).

$$P_1' = P_1\frac{(4(\cos(\phi-\phi_0)+\sin(\theta))^2 - 4\cos^2(\theta)\sin^2(\phi-\phi_0))}{(2+\sin(\theta-\phi+\phi_0)+\sin(\theta+\phi-\phi_0))^2} - P_2\frac{8\cos(\theta)\sin(\phi-\phi_0)(\cos(\phi-\phi_0)+\sin(\theta))}{(2+\sin(\theta-\phi+\phi_0)+\sin(\theta+\phi-\phi_0))^2} \tag{2.2.1a}$$

$$P_2' = P_2\frac{(4(\cos(\phi-\phi_0)+\sin(\theta))^2 - 4\cos^2(\theta)\sin^2(\phi-\phi_0))}{(2+\sin(\theta-\phi+\phi_0)+\sin(\theta+\phi-\phi_0))^2} + P_1\frac{8\cos(\theta)\sin(\phi-\phi_0)(\cos(\phi-\phi_0)+\sin(\theta))}{(2+\sin(\theta-\phi+\phi_0)+\sin(\theta+\phi-\phi_0))^2} \tag{2.2.1b}$$

$$P_3' = P_3 \tag{2.2.1c}$$

where θ and ϕ are the spherical polar angles of emission and ϕ_0 is the azimuthal angle of the detector in the x–y plane.

The corrections in equations (2.2.1) have been applied to all data from the Monte Carlo simulations.

2.3. The gas jet

The density distribution from the gas jet is assumed to be an effusive or a variant of an effusive source. The source of the gas jet is assumed to be a cylindrical pipe, one end of which is held at a driving pressure of between 10 mTorr and 50 Torr. The other end of the pipe is treated as an aperture in a thin wall separating the gas source from a perfect vacuum. Except in determining the total flux, the length of the pipe is assumed not to influence the form of the distribution. The gas jet is located along the negative y-axis. At a distance R and angle θ from the end of a pipe of cylindrical radius r_0 and gas driving pressure P_{drive}, the effusive gas pressure is:

$$P^{eff}(R,\theta) = k_{length}\frac{P_{drive}}{2\pi} \times \int_0^{\pi}\int_0^{r_0} \frac{R\cos(\theta) r\,\mathrm{d}r\,\mathrm{d}\delta}{(r^2+R^2-2rR\sin(\theta)\cos(\delta))^{3/2}}. \quad (2.3.1)$$

To reproduce experimentally observed gas profiles, $\cos^n(\theta)$ density profiles were trialled. With this distribution, the gas pressure is:

$$P_n^{eff}(R,\theta) = k_{length}\frac{(n+1)P_{drive}}{4\pi} \times \int_0^{\pi}\int_0^{r_0} \frac{R^n\cos^n(\theta) r\,\mathrm{d}r\,\mathrm{d}\delta}{(r^2+R^2-2rR\sin(\theta)\cos(\delta))^{1+n/2}}. \quad (2.3.2)$$

k_{length} is a factor, found tabulated in many sources (e.g. Loeb 1961), to correct the total flux for the finite ratio of pipe length to pipe radius. For large values of the ratio of tube length to radius, Loeb gives the following formula for k_{length}:

$$k_{length} = \frac{8r_0}{3L} \quad (2.3.3)$$

where L is the length of the gas jet.

The gas pressure at the interaction region is linearly related to the driving pressure behind the gas jet (experimentally verified by Wang *et al* (1998) for a very large pressure range). For the gas jets used in this paper, the pressures are:

$$P_{centre}(\text{gas jet 1}) = 2.48\times10^{-3}k_{length}P_{drive} \quad (2.3.4a)$$

$$P_{centre}(\text{gas jet 2}) = 9.78\times10^{-3}k_{length}P_{drive} \quad (2.3.4b)$$

$$P_{centre}(\text{gas jet 3}) = 9.74\times10^{-4}k_{length}P_{drive}. \quad (2.3.4c)$$

In figure 2, the $\cos(\theta)$ and $\cos^7(\theta)$ gas distributions are compared with the experimental results of Buckman *et al* (1993). Buckman *et al* used a cylindrical Pyrex glass tube of 1.0 mm diameter, length 15 mm and a backing pressure of 0.98 Torr. To compare with the pressures quoted later in this paper, and using the value of k_{length} implied by equation (2.3.3), this is equivalent to a pressure in this paper of around 0.09 Torr.

The effusive source is a poor representation of physical reality, but it is studied as a worst case. A $\cos^7(\theta)$ distribution, while imperfect, reflects reality a little better.

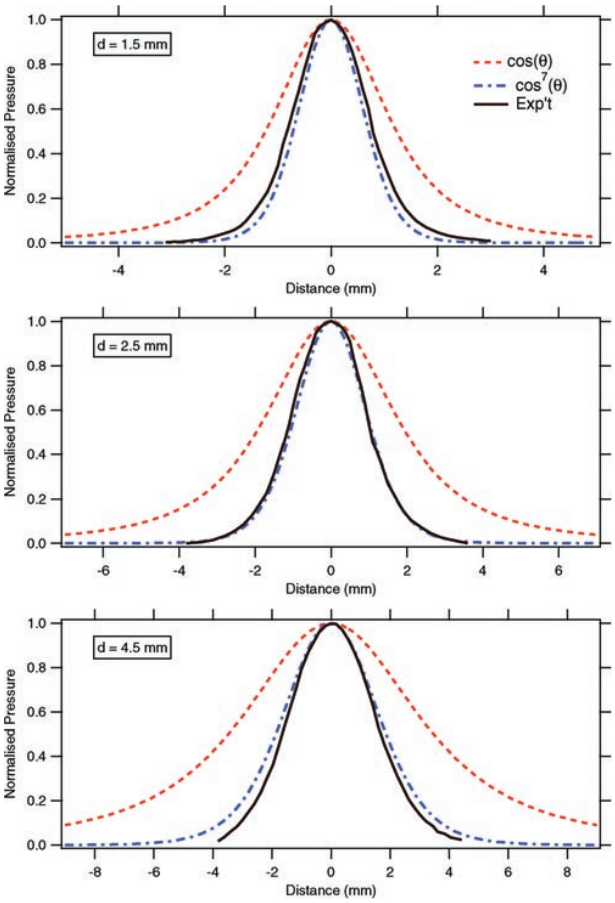

Figure 2. The experimental results of Buckman *et al* (1993) compared with two models of the pressure produced by a gas jet at three different distances from the exit of the gas nozzle. The curve labelled '$\cos(\theta)$' is a normal effusive distribution, '$\cos^7(\theta)$' is a distribution following a $\cos^7(\theta)$ law and 'Exp't' are the experimental results. All results were for a tube of diameter 1.0 mm. The experimental results were for a capillary length of 15 mm.

2.4. The absorption coefficient

The mean absorption coefficient, averaged over the Maxwellian Doppler spread, is assumed to take the following form (applicable only to low photon intensity—Wang *et al* 1998):

$$\bar{a} = \frac{1}{16\pi^{3/2}}\frac{g_2}{g_1}\frac{P\lambda_0^3\sqrt{M}}{(kT)^{3/2}\tau} \quad (2.4.1)$$

where λ_0 is the centre wavelength of the transition, g_2 and g_1 are the statistical weights of the upper and lower states respectively, T is the temperature, M the atomic mass, τ the natural lifetime of the transition, P the pressure of the absorbing medium and k the Boltzmann constant.

2.5. Modelling the trapping of resonant radiation

In this section, the results of the Monte Carlo simulation are compared with a popular theoretical model for the trapping of resonant radiation (D'Yakonov and Perel 1965, Williams *et al* 1992).

In this model it is assumed that each rank of the 'statistical tensors' (Blum 1996) representing the atomic charge distribution decays with its own characteristic rate. In the absence of other atoms, these rates are identical, but where other atoms are present and can absorb the radiation released in the studied transitions, the rates are distinct.

The decay rates of rank k multiples are:

$$\gamma_k = \gamma_0(1 - A_k\eta). \tag{2.5.1}$$

Here η is the absorption probability, which depends on gas density and interaction region geometry, γ_0 is the decay rate for an isolated atom and A_k are coefficients dependent only on the nature of the atomic states. In an unbounded medium (D'Yakonov and Perel 1965), and for a transition from total angular momentum $j_1 = 1$ to $j_0 = 0$, $A_0 = 1$, $A_1 = 0.5$ and $A_2 = 0.7$. These values have been substituted into all subsequent expressions.

The Stokes' parameters, P_x^{trap}, for a $j_1 = 1$ to $j_0 = 0$ transition are in this scheme given in terms of the untrapped parameters, P_x^0, by:

$$P_1^{trap} = \frac{10P_1^0(1 + P_4^0)(1 - \eta)}{10 - (7 - P_1^0)\eta + P_4^0(10 - (9 + P_1^0)\eta)} \tag{2.5.2a}$$

$$P_2^{trap} = \frac{10P_2^0(1 + P_4^0)(1 - \eta)}{10 - (7 - P_1^0)\eta + P_4^0(10 - (9 + P_1^0)\eta)} \tag{2.5.2b}$$

$$P_3^{trap} = \frac{2P_3^0(1 + P_4^0)(1 - \eta)(10 - 7\eta)}{(2 - \eta)(10 - (7 - P_1^0)\eta + P_4^0(10 - (9 + P_1^0)\eta))} \tag{2.5.2c}$$

$$P_4^{trap} = \frac{10P_4^0(1 + P_1^0)(1 - \eta)}{10 - (7 - P_4^0)\eta + P_1^0(10 - (9 + P_4^0)\eta)}. \tag{2.5.2d}$$

The results of these equations are labelled 'D & P' in figure 9.

These expressions take on particularly simple forms for small values of η and for $P_4^0 = 1$.

$$P_1^{trap} = P_1^0(1 - \eta/5) + \mathrm{O}(\eta^2) \tag{2.5.3a}$$

$$P_2^{trap} = P_2^0(1 - \eta/5) + \mathrm{O}(\eta^2) \tag{2.5.3b}$$

$$P_3^{trap} = P_3^0(1 - 2\eta/5) + \mathrm{O}(\eta^2) \tag{2.5.3c}$$

$$P_4^{trap} = 1 - \frac{2\eta}{5(1 + P_1^0)} + \mathrm{O}(\eta^2). \tag{2.5.3d}$$

Equation (2.5.3d) implies a very rapid variation of P_4^{trap} with pressure as P_1^0 approaches -1. An example of this behaviour can be seen in figure 7.

For comparison, another simple model of trapping is considered. In this model, the exact weak field equations are integrated over all angles of absorption.

The angle averaged Stokes parameter P_j emitted after 'i' absorptions is denoted $P_j^{(i)}$.

With the assumption that the probability of absorption within the gas cell can be written as $\eta = (1 - \exp(-k_{abs}\,p))$, where p is the gas pressure and k a proportionality factor, and that the probability of 'i' absorptions is $\exp(-k_{abs}\,p)(k_{abs}\,p)^i/i!$, the net polarization can be written:

$$P_j = \exp(-k_{abs}\,p)\sum_{i=0}^{\infty}\frac{(k_{abs}\,p)^i}{i!}P_j^{(i)}. \tag{2.5.4}$$

3. The Monte Carlo simulation

3.1. Introduction

An excitation point is generated at random from the product of the effusive gas jet distribution and the Gaussian electron beam profile. Photons are released at times according to the $\mathrm{e}^{-t/\tau}$ distribution, into angles reflecting the intensity distribution defined by the electron excited state. Once released, the first step is to decide whether the photon results from the transition to the 2^1S state (visible 501.6 nm photons) or to the 1^1S state (UV 53.7 nm photons). If it has decayed to the former state, it will not be absorbed again, and if it has decayed to the latter state, it can be absorbed again by ground state atoms. The branching ratios to the 2^1S and 1^1S states are $b_2 = 0.023$ and $b_1 = 0.977$ respectively (Hishikawa *et al* 1992). For UV photons, the gas density is integrated along the photon's direction of propagation to determine whether the photon is absorbed. If the photon is not absorbed, it is free to travel to the detector. If it reaches the detector it is counted, and if it does not, it is discarded. If absorbed, the absorbing atom then releases another photon with an intensity distribution determined by the polarization and propagation angle of the absorbed photon. The process is repeated until a photon is not absorbed and is free to be counted.

Figure 3 shows a flowchart depicting this process.

3.2. Generating the probability distributions

Quasi-random uniform distributions can be easily generated with modern computing packages. The random number generator should be chosen as a compromise between quality and CPU overhead. The current work uses the real and integer random number generators built into *Mathematica*. These generators have been found acceptable for over 10^6 random numbers. This exceeds the maximum number of random numbers used in any calculation in this paper.

To generate a non-uniform distribution, a transformation is applied to the uniform distribution. If ξ is a random number distributed uniformly over the interval [0, 1], and $P(x)$ is the distribution one wishes to reproduce, where $x \in [x_0, x_1]$, then the function $\mathrm{CPF}^{-1}(\xi)$ gives the desired distribution, where $\mathrm{CPF}(x)$ (or the cumulative probability function) is given by:

$$\mathrm{CPF}(x) = \left(\int_{x_0}^{x} P(x)\,\mathrm{d}x\right)\left(\int_{x_0}^{x_1} P(x)\,\mathrm{d}x\right)^{-1}. \tag{3.2.1}$$

Extensions to two or more dimensions are given in any elementary statistical text (e.g. Shreider 1964).

As an example, points distributed with spherical symmetry can be assigned the spherical polar angles $\phi = 2\pi\xi$ and $\theta = \cos^{-1}(1 - 2\xi)$.

Table 1. Apertures and solid angles used in the detectors. θ_a is the acceptance angle, Ω the solid angle and θ_0 the opening angle, as illustrated in figure 4.

	d (mm)	s (mm)	r_1 (mm)	r_2 (mm)	θ_a (°)	Ω (sr)	θ_0
Large solid angle	30	20	60	60	50.2	2.26	80.5°
Small solid angle	30	20	11	17.5	19.3	0.353	54.9°

Table 2. Stokes' parameters used in this paper.

Data set	State	Impact energy (eV)	Scattering angle (°)	P_1	P_2	P_3	P_4	Reference
1	He 3^1P	29.6	50	−0.092	−0.9586	−0.2694	1	Fon *et al* (1991)
2	He 3^1P	80	40	0.2926 ± 0.017	-0.0143 ± 0.0347	-0.956 ± 0.013	1	Beijers *et al* (1987)
3	Hg 6^1P_1	100	10	−0.9338	0.0783	−0.3495	0.9864	McEachran (private commun.)

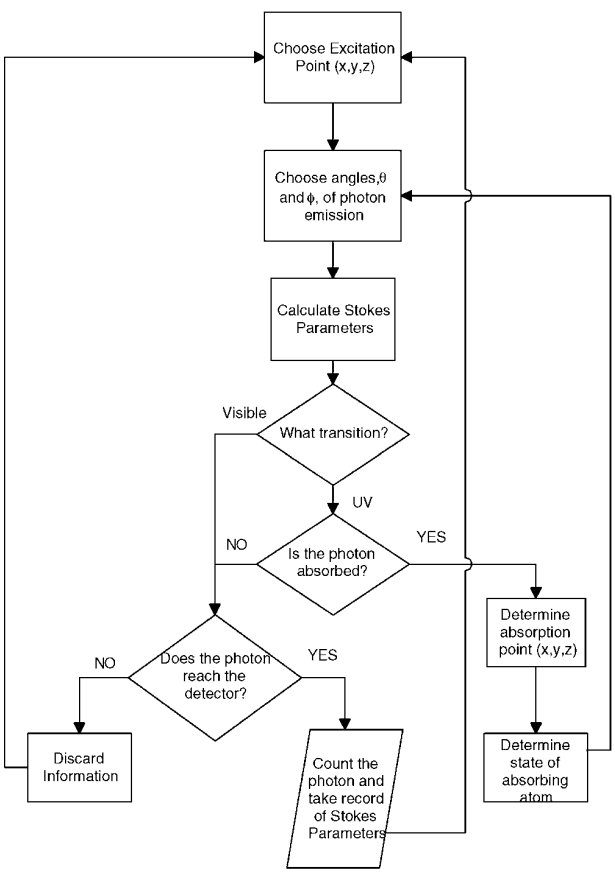

Figure 3. A flowchart illustrating the chain of processes and decisions in the Monte Carlo routine.

Table 3. The electron beam widths, gas jet dimensions and gas distribution forms used in this paper.

Gas jet	Γ (mm)	d (mm)	r_0 (mm)	n
1	1	1.5	0.15	1
2	1	1.5	0.15	7
3	2.35	4	0.25	1
4	uniform pressure $60 \times 60 \times 60$ mm^3			

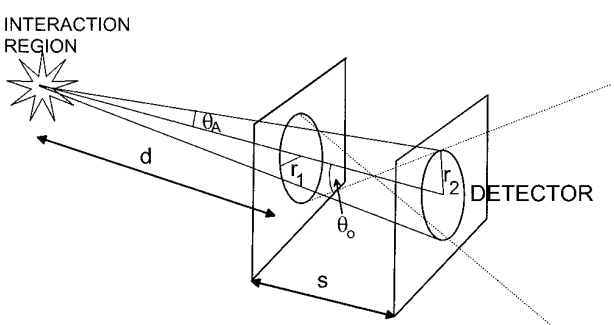

Figure 4. Parameters used in the definition of a detector in this paper. The detector consists of two circular apertures of radius r_1 and r_2 separated by a distance s, the first of which is a distance d from the centre of the interaction region. The acceptance angle, $\theta_a = \min(\arctan(r_2/(d+s)), \arctan(r_1/d))$, is half the collection angle, and is related to the solid angle, Ω, by $\Omega = 2\pi(1-\cos(\theta_a))$. The opening angle, $\theta_0 = \arctan((r_1+r_2)/s)$, determines how much of the background gas is seen by the detector.

It is only the rare distribution that will yield to this simple analysis. In general, the inverse of the CPF cannot be analytically constructed.

Once a photon is released in the interaction region there is a possibility that it will be subsequently absorbed and re-emitted. If the gas density and absorption probability are constant, the distributions can be constructed easily. If a photon travels along the x axis from $x = 0$, and the constant mean free path is λ, the distribution of absorption points is described by $x(\xi) = -\lambda \ln(\xi)$.

Where the density is not uniform or equivalently where the mean free path is position dependent, the probability of absorption in the range $[x, x + \mathrm{d}x]$ after travelling uninterrupted from the point x_i is:

$$P_{abs}(x)\,\mathrm{d}x/\lambda(x) = \exp\left(-\int_{x_i}^{x} \frac{\mathrm{d}x'}{\lambda(x')}\right)\mathrm{d}x/\lambda(x). \quad (3.2.2)$$

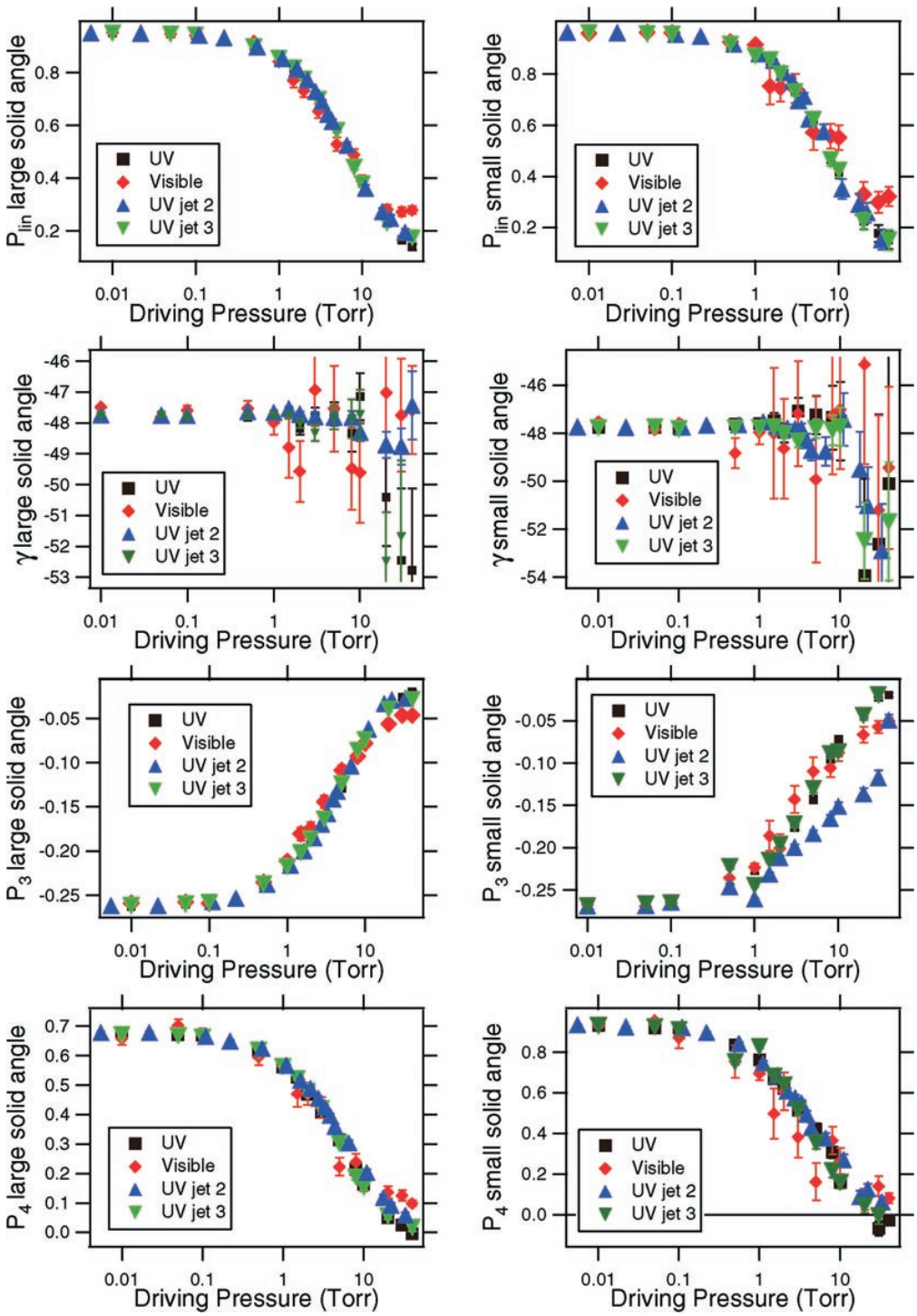

(a)

Figure 5. The coherence parameters, P_{lin}, γ, P_3 and P_4, versus the driving pressure behind the gas jet for data set 1. Unless declared otherwise, gas jet 1 was used. For illustrative purposes only, a scaling factor of 2.2 was used for the pressure of gas jet 2. In this and all subsequent diagrams, γ is in degrees. (b) The coherence parameters, P_{lin}, P_3 and P_4, versus a smaller range of driving pressures. Gas jets 1 and 2 are depicted for data set 1. The pressure in jet 2 has been scaled by a factor of 2.2. The curves labelled D & P are the results of the D'Yakonov–Perel theory examined in section 2.5. It has been assumed that $k_{abs} = 0.41$. The data are for the small solid angle detector only.

To generate the distribution, one should solve:

$$\int_{x_i}^{x} \frac{\mathrm{d}x'}{\lambda(x')} = -\ln(\xi) \qquad (3.2.3)$$

for $x \equiv x(\xi)$.

However, if

$$\xi < \exp(-\int_{x_i}^{x_{max}} \frac{\mathrm{d}x'}{\lambda(x')}),$$

the photon is not absorbed, and may proceed to the detector.

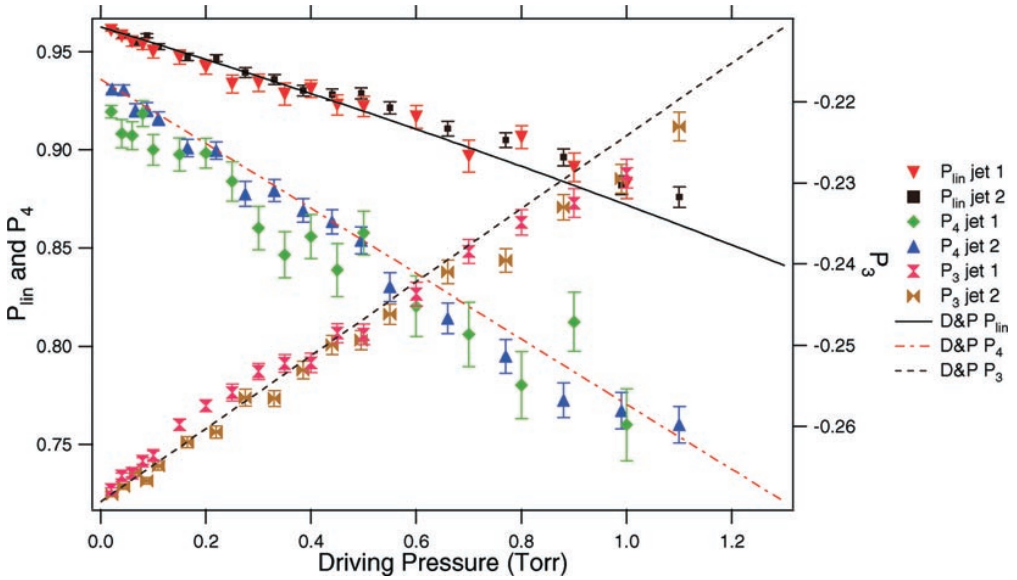

(b)

Figure 5. (Continued)

3.3. Monte Carlo run parameters

Table 1 lists the two detectors used in this work. The large solid angle detector is not meant to be physically realistic, and features an unfeasibly large solid angle of 2.26 sr. It has been included to produce parameters with reduced statistical uncertainty. The small solid angle detector still features a relatively large solid angle of 0.35 sr.

Three data sets are used in this analysis: one is from a theoretical analysis of the electron excited He 3^1P state (Fon *et al* 1991), the second is from an experimental study of the same state (Beijers *et al* 1987) and the final set is taken from a theoretical analysis of the electron excited Hg 6^1P_1 to 6^1S_0 transition (McEachran 1994, private communication). The Stokes parameters are listed in table 2.

Three gas jets are used in the analysis. These are defined in table 3. The variables are Γ, the spatial full width at half maximum of the electron beam, d, the distance of the end of the gas jet from the interaction centre, r_0, the radius of the gas jet cylinder, and n, giving the value of the exponent in the assumed form of the distribution, $\cos^n(\theta)$. For an effusive source, $n = 1$. As discussed in section 2.3, $n = 7$ was studied to improve the agreement with observed gas jets.

In addition, the code was run using a region of uniform pressure. In this model, the points of initial electron excitation were randomly and uniformly spread throughout a rectangular prism of extent along the x, y and z axes of 20 mm, 20 mm and 60 mm respectively. The radiation could then be trapped in a region of 60 mm $\times$ 60 mm $\times$ 60 mm. In this model, it is assumed that the gas jet cylinder offers no obstruction to the light.

4. Sources of error

There are several deficiencies and sources of error in the model. The electrons are presumed to travel collinearly through the entire interaction region with no misalignment or range of pencil angles. No account is made for the restrictions imposed by the finite solid angle of the electron detector. Emissions and absorptions are handled exactly, but the implementation involves numerical approximations. The gas jet is not physically realistic, and is confined to a very finite region.

There are also computational deficiencies imposed by the available time and the memory restrictions of the computer. For each pressure, the number of iterations was between 30 000 and 100 000, which introduced statistical problems for small solid angles. Inverses of probability distributions were for the most part produced by interpolating functions evaluated on a grid. To keep within the memory boundaries of the machine, the grid was made as coarse as was consistent with a satisfactory emulation of the original probability distribution. This coarseness causes problems particularly at the edges of distributions, and most particularly when the probability approaches zero. Having said this, the probability distribution of the first photon emission after electron excitation is handled very accurately, and so especially for small gas pressures the results are expected to be very reliable.

Another potential source of error is the artificial boundary imposed upon the interaction region. To keep the calculations manageable, the distribution of electron excitation centres and the gas density distribution are set to zero beyond, and sometimes well beyond, the point at which the probability drops below 1% of the peak probability. This precludes excitations or resonant absorption due to the background gas or from the extreme tails of the distributions of the gas jet and electron beam. This may give rise to serious errors at larger pressures.

The effects of any change in electron scattering angle are ignored in this study. This is equivalent to assuming that the distance of the electron detector from the scattering centre is very much greater than the dimensions of the scattering centre. For small scattering angles, the effects of changes in the scattering angle and scattering plane can be very large (Zetner *et al* 1990, van der Burgt *et al* 1991).

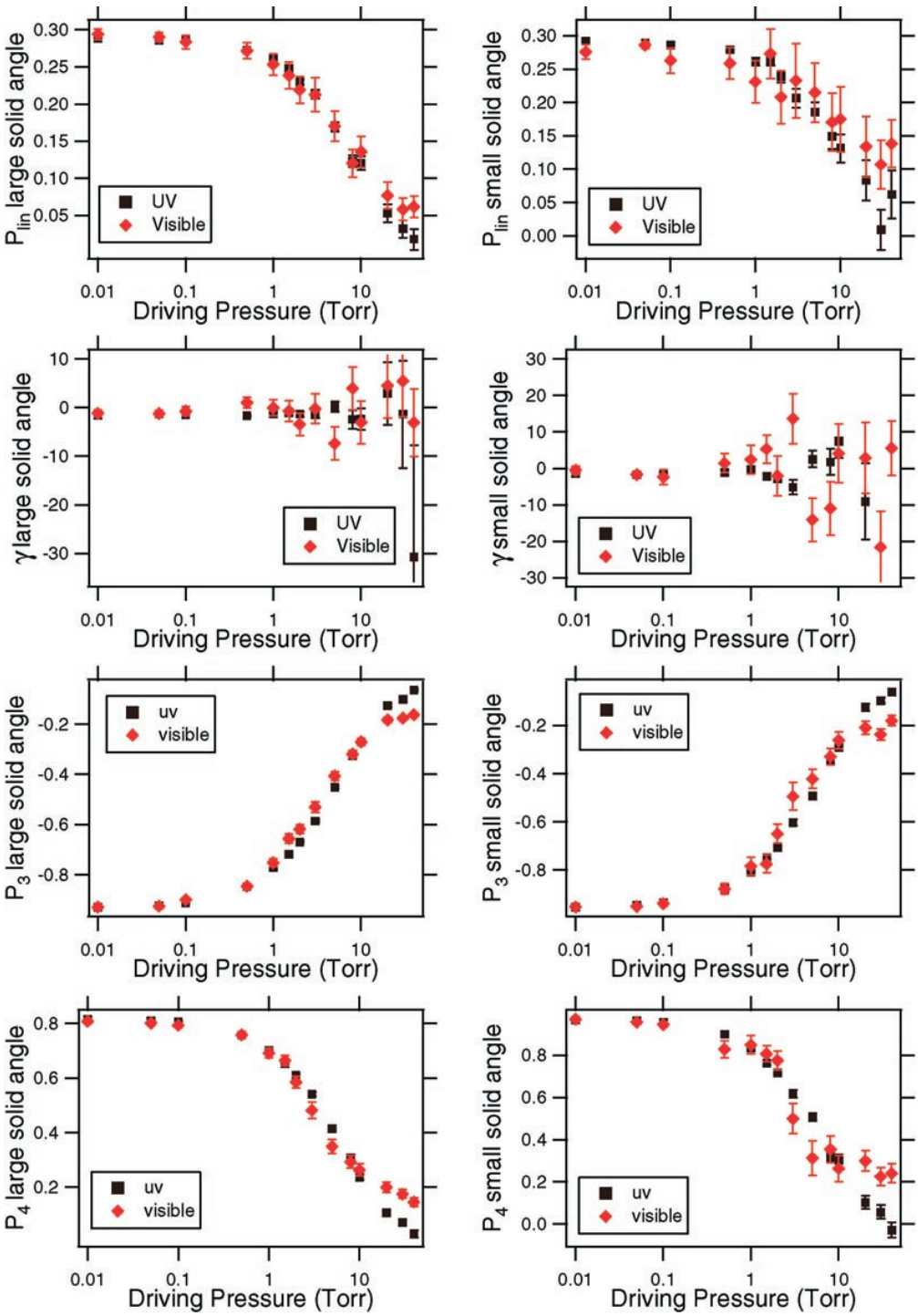

Figure 6. The coherence parameters, P_{lin}, γ, P_3 and P_4, versus the driving pressure behind the gas jet for data set 2 and gas jet 1.

All the error bars in this work are estimates of one standard deviation. Where error bars are not shown, they are smaller than the marker used in the plot.

5. Results

The principal results of this paper are presented in figures 5–7. These show the Andersen parameters, P_{lin} and γ, and the Stokes parameters P_3 and P_4 as a function of the pressure behind the gas jet for the three data sets, and for the three gas jet models.

The Andersen parameters (Andersen *et al* 1988) carry more obvious physical significance than the Stokes parameters. $L_\perp$, P_{lin}, γ and ρ_{00} are the angular momentum transferred to the atom, linear polarization of the charge cloud, angular orientation of the charge cloud and height of the charge cloud normal to the scattering plane respectively. Since $L_\perp = -P_3$, P_3 was plotted rather than $L_\perp$, and it was

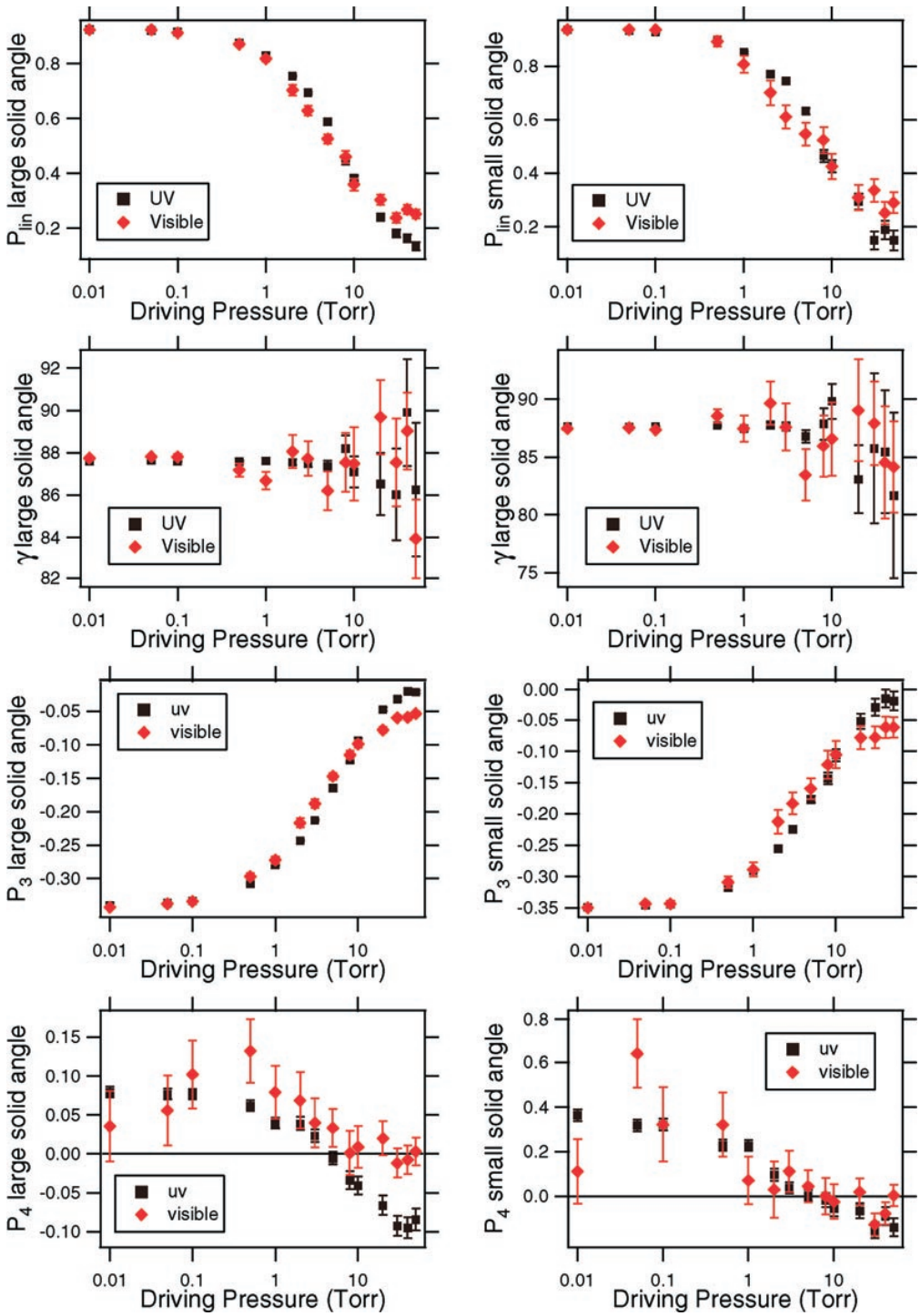

Figure 7. The coherence parameters, P_{lin}, γ, P_3 and P_4, versus the driving pressure behind the gas jet for data set 3 and gas jet 1.

chosen to plot P_4 rather than its closely related parameter ρ_{00}, where $\rho_{00} = (1 + P_1^0)(1 - P_4^0)/[3 + P_4^0 + P_1^0(1 - P_4^0)]$ and where $\rho_{00} = 0$ corresponds to $P_4 = 1$.

To correct the pressures for a gas jet of finite length, the pressures in the ordinate should be multiplied by a factor of $1/k_{length}$. As will be discussed in more depth later, to reproduce the experimental data of Mikosza *et al* (1994) the pressure of gas jets 1 and 3 had to multiplied by a factor of 8.5 ± 1.0, and the pressure in gas jet 2 by a factor of 19.0 ± 2.0.

In determining the pressure corrected polarizations from experimental measurements, one needs to be able to relate the absorption probability to the pressure. In the model of D'Yakonov and Perel (1965), the decay rate falls as $\gamma_0(1 - \eta)$. Equivalently, the lifetime rises linearly with absorption probability as $\tau_0(1 + \eta)$. If the decay rate or lifetime is plotted against pressure, the slope reveals the relationship between pressure and absorption probability.

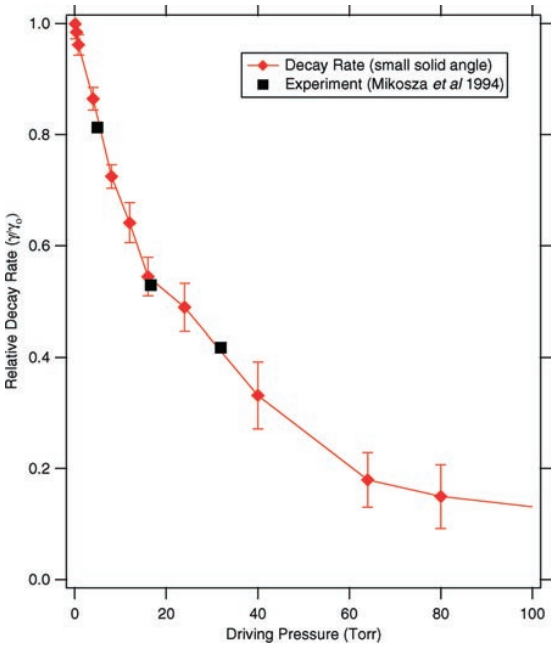

Figure 8. A comparison between the decay rates of the Monte Carlo simulation for data set 1 with small solid angle, and the experimental measurements of Mikosza *et al* (1994) for the 3^1P to 1^1S transition. The pressures for the Monte Carlo data have been scaled to the experimental pressures.

Table 4. Approximate percentage changes in polarization at 1 Torr driving pressure. Gas jet 1 is used throughout.

Data set	P_1	P_2	P_3	P_4
1	−13%	−10%	−15%	−17%
2	−5%	—	−9%	−7%
3	−5%	−9%	−9%	−21%

The relationship between absorption probability, η, and the pressure, p, is of the form $\eta = k_{abs}\,p$ for small values of p. For gas jets 1 and 3, $k_{abs} = 0.413 \pm 0.006$, and for gas jet 2, $k_{abs} = 0.98 \pm 0.02$.

The theory of D'Yakonov and Perel (1965) predicts pressure dependent values of the relaxation rates of intensity, orientation and alignment. According to equation (2.5.1), the lifetimes of intensity, orientation and alignment are $\tau_{int}/\tau_0 = 1/(1-\eta)$; $\tau_{orient}/\tau_0 = 1/(1-0.5\eta)$ and $\tau_{align}/\tau_0 = 1/(1-0.7\eta)$. An analysis of the data demonstrates that the lifetimes do differ. However the linear fits to the low pressure end of data set one indicate that the slope of the orientation and alignment curves are not 0.5 and 0.7 as predicted by theory, but 0.349 ± 0.025 and 0.633 ± 0.026 respectively. A more thorough analysis of a range of Stokes parameters was used to independently establish values for the A_k coefficients of equation (2.5.1). Using gas jet 1 at a single driving pressure of 1 Torr it was found that $A_1/A_0 = 0.474 \pm 0.004$ and $A_2/A_0 = 0.713 \pm 0.006$ for the large solid angle detector

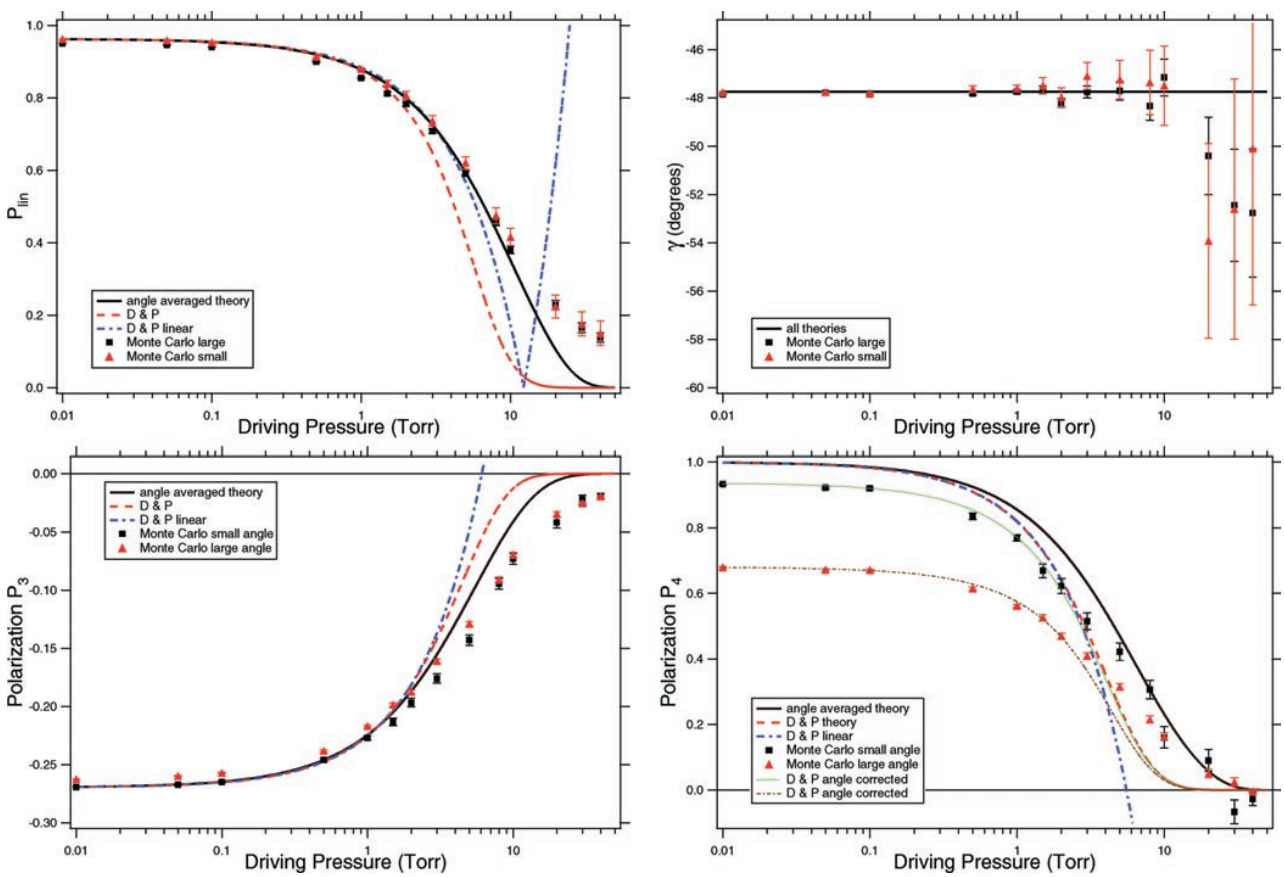

Figure 9. Various models for radiation trapping for data set 1. For details, refer to the text. The Monte Carlo calculations used gas jet 1. Only the UV data have been plotted.

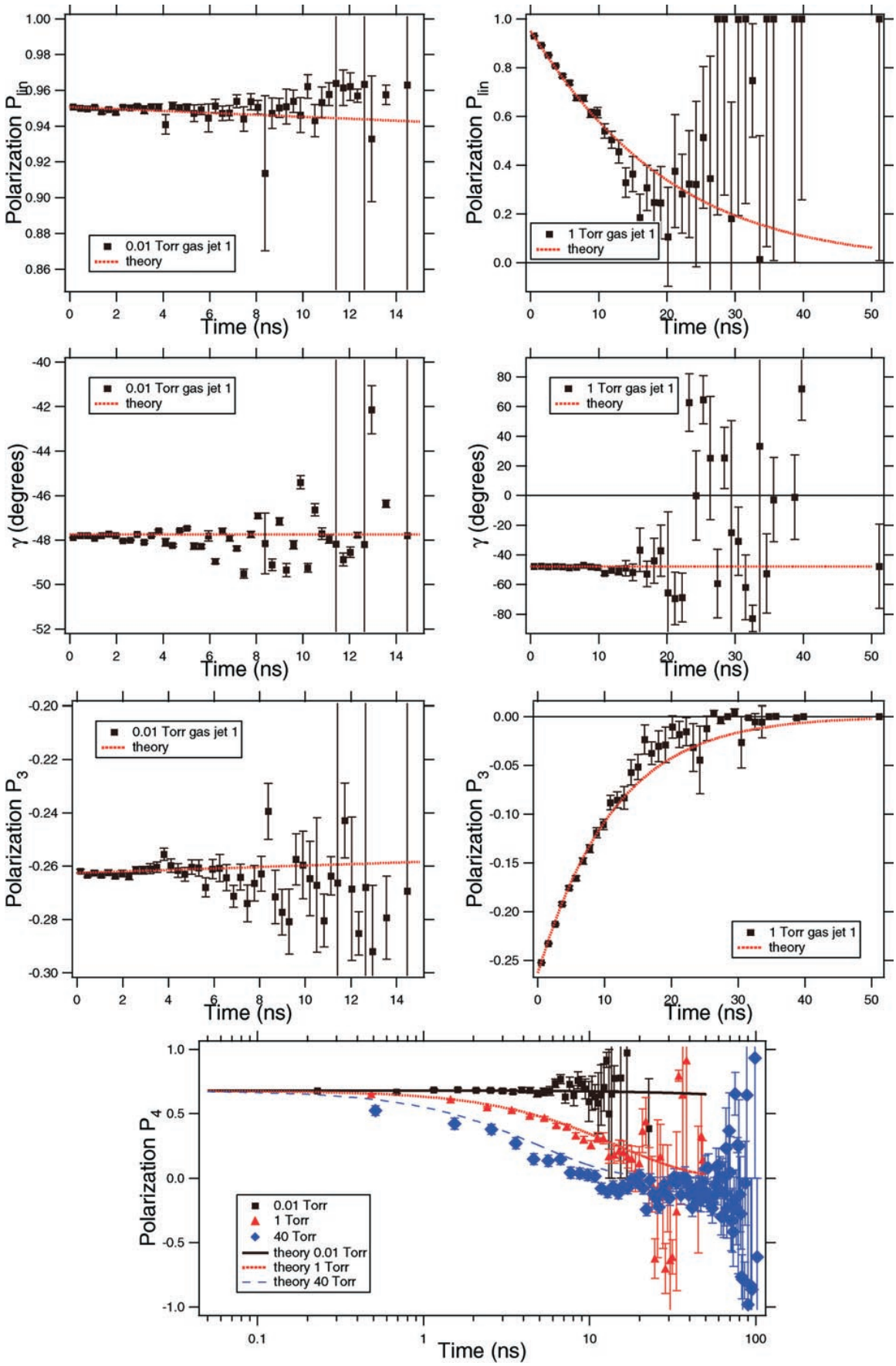

Figure 10. The parameters, P_{lin}, γ, P_3 and P_4 as a function of decay time for driving pressures of 0.01 Torr and 1 Torr and 40 Torr for data set 1 and gas jet 1. The theory is the solid angle integrated model of D'Yakonov–Perel (1965) for $k_{abs} = 0.41$.

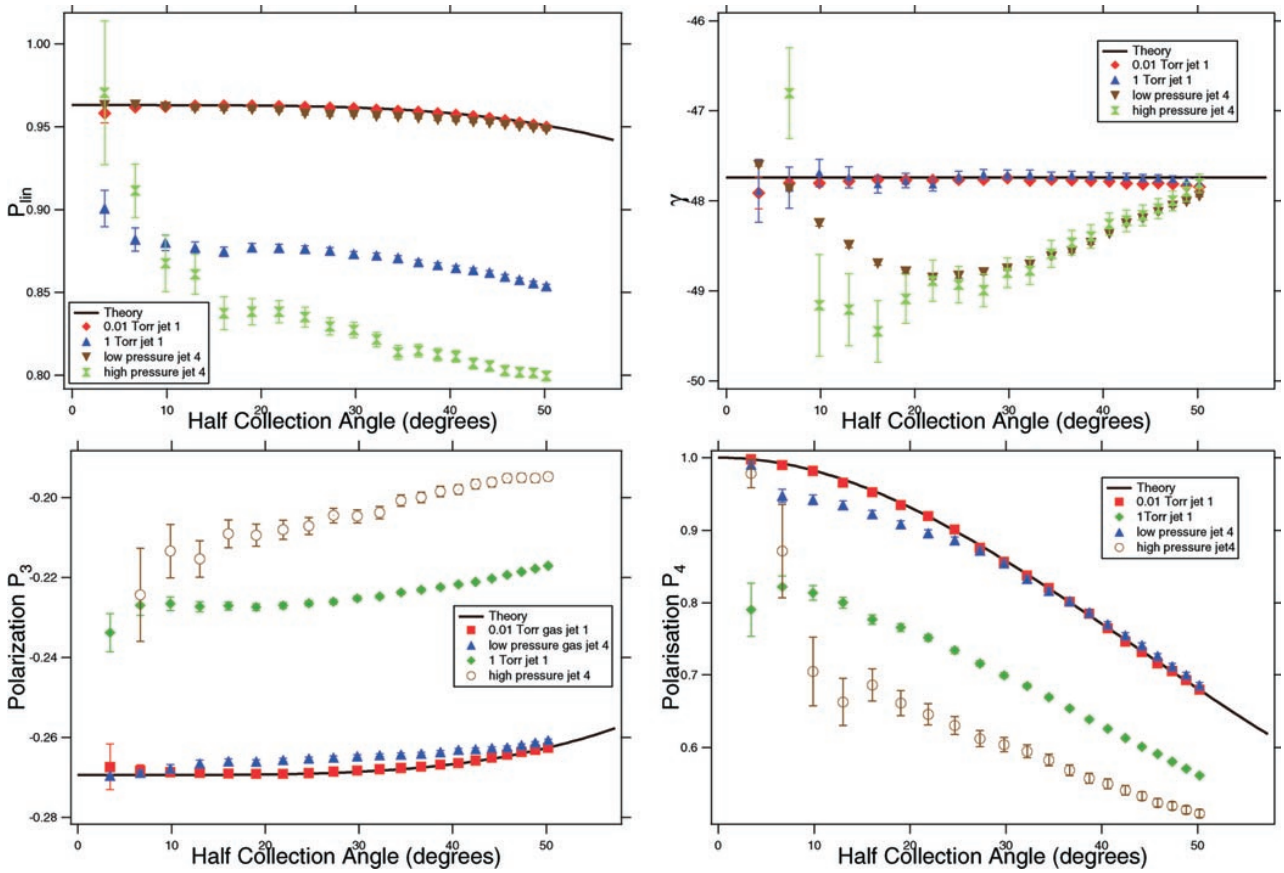

Figure 11. The parameters, P_{lin}, γ, P_3 and P_4, as a function of the acceptance angle (or half the collection angle) of the detector. Only data set 1 and gas jets 1 and 4 are considered. Low and high pressures for gas jet 4 are 1.6×10^{-6} Torr and 1.6×10^{-4} Torr respectively through the interaction region.

and $A_1/A_0 = 0.495 \pm 0.009$ and $A_2/A_0 = 0.764 \pm 0.016$ for the small solid angle detector. The errors quoted are derived from weighted averages of many fits to the lifetime data. The data had wide variations and the errors may well be underestimated.

Figure 8 shows a comparison between the experimental decay rate data of Mikosza *et al* (1994) and the Monte Carlo results for data set 1 for the small solid angle detector. Since the pressures have to be scaled, the agreement of the two cannot be said to vindicate the Monte Carlo results. The most that can be said is that the calculations are not inconsistent with experiment. The scaling factors of 8.5 ± 1.0 for gas jets 1 and 3, and 19 ± 2.0 for gas jet 2, imply a gas jet length to radius ratio of about 23 ± 3 and 51 ± 5 respectively. Mikosza *et al* (1994) do not state a value for the length to radius ratio of their gas jet, but Humphrey *et al* (1987) used a length to radius ratio of about 64. If this ratio is similar to that of the gas jet used in these experimental measurements, this is an indication that gas jet 2 produces a gas distribution closest to reality.

In figure 9, the two radiation trapping models discussed in section 2.5 are compared with the UV data from the Monte Carlo calculations for data set 1. The curves marked 'angle corrected' are the only curves corrected for finite solid angle. The curves marked 'D & P' (equations (2.5.2)) and 'D & P angle corrected' use an approximation that the probability of absorption, η, can be written in terms of k_{abs} and p as $\eta = (1 - \exp(-k_{abs}\, p))$. The linear curves (equations (2.5.3)) assume that $\eta = k_{abs}\, p$. In all cases, it is assumed that $k_{abs} = 0.41$. The 'angle averaged theory' uses equation (2.5.4).

The Monte Carlo data can be analysed as a function of the time following the moment of excitation. This information can also be extracted from experimental data, as shown by Mikosza *et al* (1994). The analysis was performed only for data set 1 and gas jet 1. Figure 10 shows the Andersen parameters P_{lin} and γ, and the Stokes parameters P_3 and P_4 as a function of time for two driving pressures. The theory has been integrated over the solid angle of the detector (the large solid angle has been used for this data) and a value of $k_{abs} = 0.41$ has been assumed.

Figure 11 shows the parameters as a function of the acceptance angle of the photon detector.

Finally, in figures 12 and 13, the Monte Carlo procedure is applied to two complete sets of data. Each set is for a single electron impact energy and the complete range of scattering angles from 0 to 170°. The data are taken from Fon *et al* (1991) for 26.5 eV and 29.6 eV excitation. The results are compared with the experimental data of Neill and Crowe (1988) and Neill *et al* (1989). For the Monte Carlo data, only the UV transition and the first gas jet have been considered.

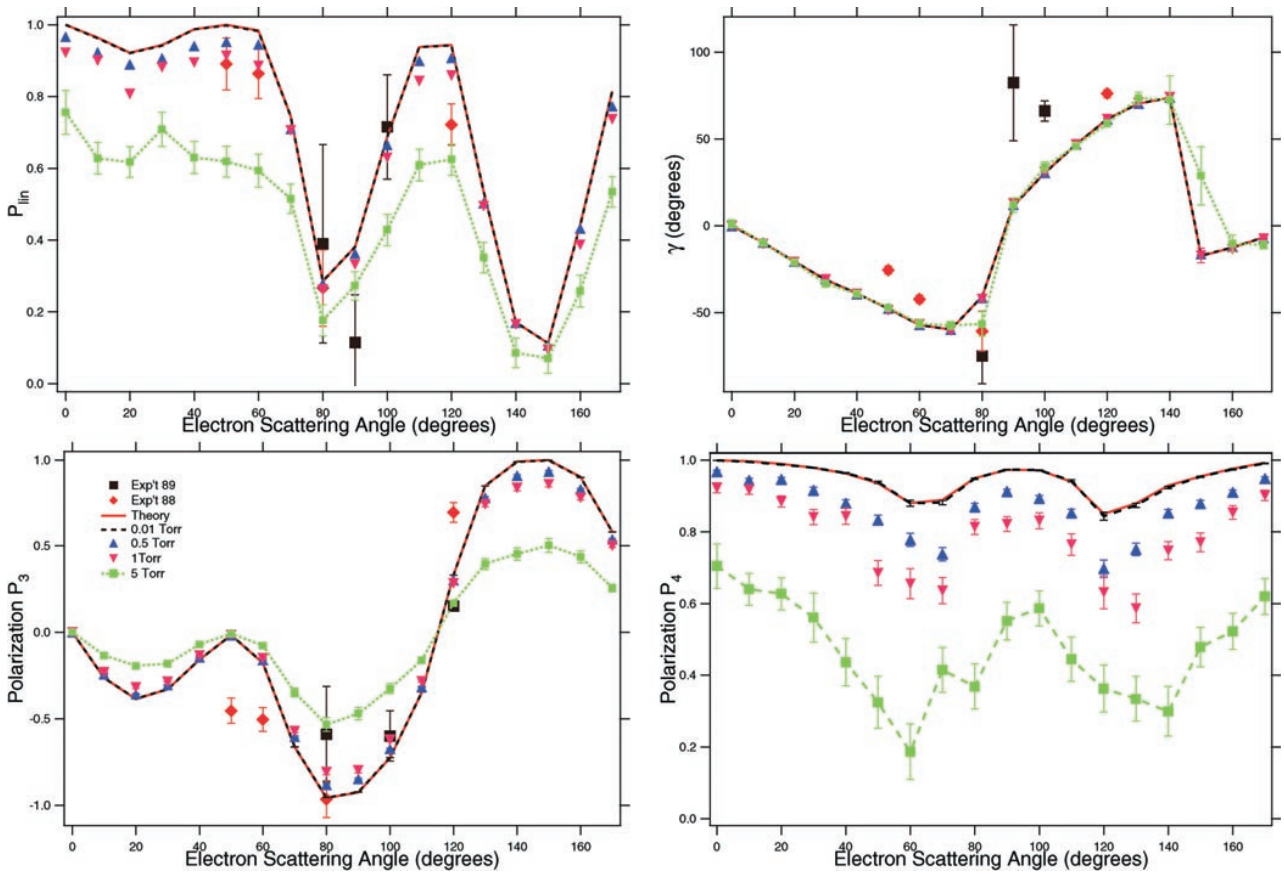

Figure 12. The effect of pressure on the parameters P_{lin}, γ, P_3 and P_4 for a complete set of electron scattering angles. The theoretical data are from the R-matrix theory of Fon *et al* (1991) for 26.5 eV electron impact excitation of the He 3^1P state. The experimental data are from Neill and Crowe (1988) and Neill *et al* (1989) and are denoted by 'Exp't 88' and 'Exp't 89' respectively. Gas jet 1 is used, and only the UV Monte Carlo data are plotted.

6. Discussion

The principal features of the data include a general tendency for the absolute value of the polarization to decrease and approach zero as the pressure rises. The alignment angle, γ, of the charge cloud appears to be independent of pressure, but the value of P_{lin} drops sharply with pressure. This suggests that the charge cloud does not rotate, but its midriff grows with pressure.

The radiation trapping correction method of Williams *et al* (1992), which is based on the theory of D'Yakonov and Perel (1965), appears to produce satisfactory results for driving pressures up to about 1 or 2 Torr (equivalent to about 9 to 17 Torr for the gas jet of Mikosza *et al* 1994), and for times up to about 10 to 15 ns after excitation.

There is a discrepancy between the current results and the experimental work of Mikosza *et al* (1994). Their experiments suggest that the alignment angle, γ, may change with pressure and time after decay. However the Monte Carlo calculations and the theory of D'Yakonov and Perel (1965) suggest that γ is constant with time and with pressure. Gas jet 4, which is a 60 mm cube of uniform pressure, was invoked principally as a test of this behaviour. It was thought that perhaps excitation of extreme points in the gas distribution might cause γ to change. However this gas distribution did not cause γ to change. It would seem that there are either some experimental factors not satisfactorily modelled by the present Monte Carlo approach, or that the rotation of the charge cloud is an artefact peculiar to the angular correlation technique.

Mikosza *et al* (1994) also suggest that the parameter P_{lin} is larger than the D'Yakonov–Perel theory predicts. Figure 9 provides clear affirmation of this finding; at greater than a few Torr, P_{lin} diverges very strongly from the theory.

Table 4 lists the very approximate percentage change in polarizations for the three data sets at a driving pressure of 1 Torr (equivalent to a real experimental pressure of between 8 and 10 Torr). Every parameter shows a substantial change, but P_4 shows a very dramatic change for the first and third data sets. P_4 is more sensitive in every way to changes in the experimental conditions, to changes in pressure and angular misalignments.

Pressure dependent effects on entire data sets are studied in figures 12 and 13. At a driving pressure of 0.5 Torr, there are very significant deviations from theory, and by 5 Torr the results are grossly distorted. However these results do not appear to explain the deviations of the experimental data from theory. This would either suggest that the theory is inadequate or that there are experimental effects not incorporated by the present analysis (such as

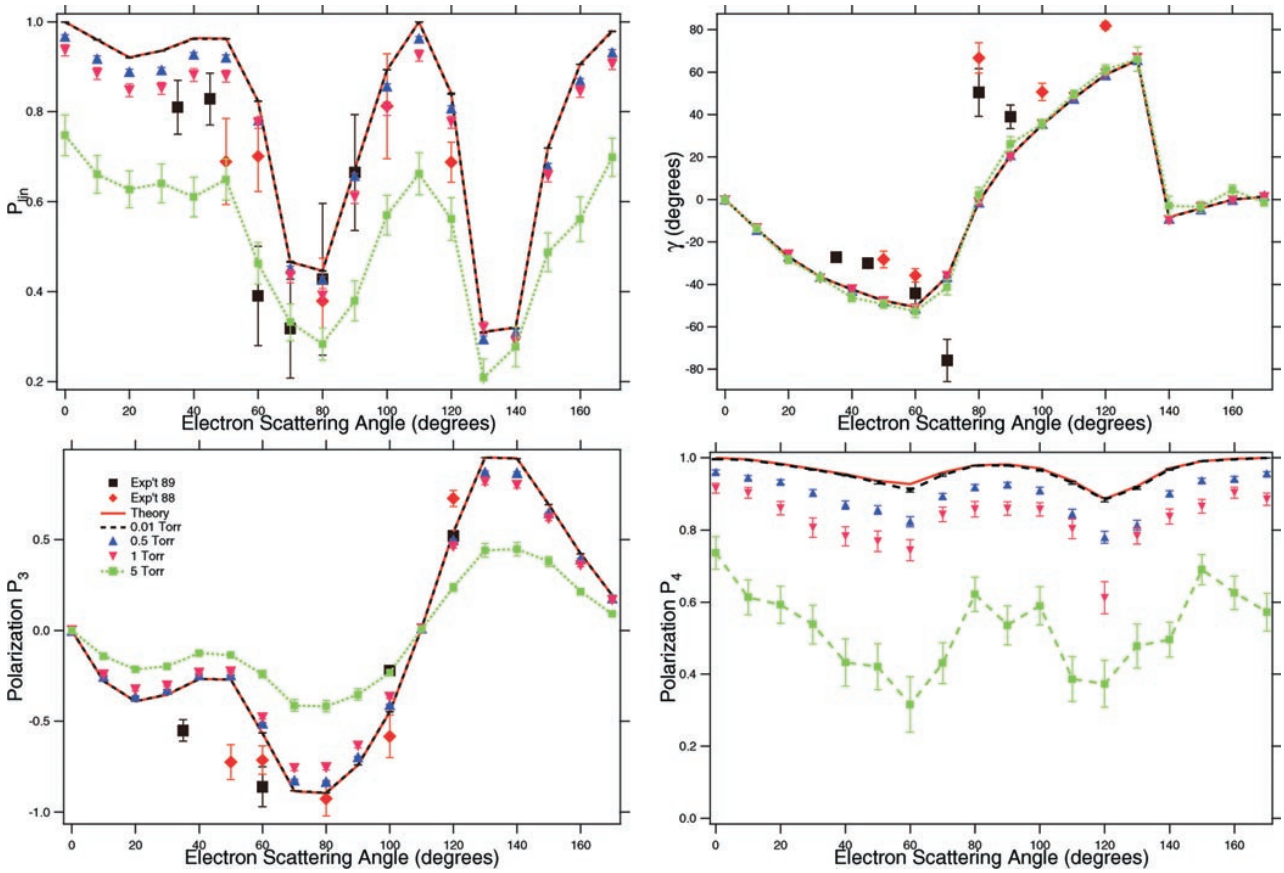

Figure 13. As in figure 12, except that the electron energy is 29.6 eV.

a realistic electron detector). Driving pressures of up to 5 Torr are insufficient to cause any major changes in the γ parameter.

For more widely applicable conclusions, there are several extensions that can be made to the current work:

- Incorporate a realistic model of the gas jet (e.g. Olander and Kruger 1970).
- Incorporate a real electron detector with a finite solid angle (to model the effect of changes in scattering plane and scattering angles due to finite excitation volume).
- Extend the borders of the gas jet and include background gas.
- Examine the angular correlation technique.
- Improve the statistics.

7. Conclusions

The study has shown that pressure dependent effects are important at even very moderate driving pressures. However, for pressures of less than about 0.1 k Torr, all parameters are only minimally affected by radiation trapping (where $k = 1/k_{length} > 1$ is a factor to correct for the length to radius ratio of the gas jet). Since k is typically between 10 and 20, this generally implies a practicable working pressure. If one must work at higher pressures (to produce sufficient intensity, for example) or if high precision is required, a correction must be applied to the data. Fortunately, the correction method of Williams *et al* (1992) has been shown to be very effective for pressures up to 1.5 k Torr, which might mean an experimental driving pressure of up to an extremely large 30 Torr.

References

Andersen N, Gallagher J W and Hertel I V 1988 *Phys. Rep.* **165** 1
Beijers J P M, Madison D H, van Eck J and Heideman H G M 1987 *J. Phys. B: At. Mol. Phys.* **20** 167
Blum K 1996 *Density Matrix Theory and Applications* 2nd edn (New York: Plenum)
Brink D M and Satchler G R 1994 *Angular Momentum* 3rd edn (Oxford: Oxford University Press)
Buckman S J, Gulley R J, Moghbelalhossein M and Bennett S J 1993 *Meas. Sci. Technol.* **4** 1143
D'Yakonov M I and Perel V I 1965 *Sov. Phys.–JETP* **20** 997
Fon W C, Berrington K A and Kingston A E 1991 *J. Phys. B: At. Mol. Opt. Phys.* **24** 2161
Hishikawa A, Mizuno H, Tani M and Okasaka R 1992 *J. Phys. B: At. Mol. Opt. Phys.* **25** 3419
Humphrey I 1999 *Meas. Sci. Technol.* **10** 403
Humphrey I, Williams J F and Heck E L 1987 *J. Phys. B: At. Mol. Phys.* **20** 367
Loeb L B 1961 *The Kinetic Theory of Gases* 3rd edn (New York: Dover)
McLaughlin D T, Baerveldt A W, McDonald D G, Crowe A, van Eck J and Heideman H G M 1994 *J. Phys. B: At. Mol. Opt. Phys.* **27** L19
Mikosza A G, Hippler R, Wang J B, Williams J F and Wedding A B 1994 *J. Phys. B: At. Mol. Opt. Phys.* **27** 1429
Neill P A and Crowe A 1988 *J. Phys. B: At. Mol. Opt. Phys.* **21** 1879

Neill P A, Donnelly B P and Crowe A 1989 *J. Phys. B: At. Mol. Opt. Phys.* **22** 1417
Olander D R and Kruger V 1970 *J. Appl. Phys.* **41** 2769
Shreider Y A 1964 *Method of Statistical Testing: Monte Carlo Method* (Amsterdam: Elsevier)
Van der Burgt P J M, Corr J J and McConkey J W 1991 *J. Phys. B: At. Mol. Opt. Phys.* **24** 1049
Wang J B, Wu H Y, Williams J F and Mikosza A G 1998 *J. Phys. B: At. Mol. Opt. Phys.* **31** 1603
Williams J F, Mikosza A G, Wang J B and Wedding A B 1992 *Phys. Rev. Lett.* **69** 757
Zetner P W, Trajmar S and Csanak G 1990 *Phys. Rev.* A **41** 5980
Zetner P W, Trajmar S, Csanak G and Clark R E H 1989 *Phys. Rev.* A **39** 6022